High Voltage Phosphate Cathodes for Rechargeable Ca-ion Batteries

Sanghyeon Kim[†,‡], Liang Yin[‡,§], Myeong Hwan Lee[ǀ], Prakash Parajuli[‡,‖], Lauren Blanc[‡,#], Timothy T. Fister[†,‡], Haesun Park[‡,Δ], Bob Jin Kwon[†,‡], Brian J. Ingram[†,‡], Peter Zapol[‡,Δ], Robert F. Klie[‡,‖], Kisuk Kang[ǀ,⊥,ζ], Linda F. Nazar[‡,#], Saul H. Lapidus[‡,§], and John T. Vaughey*[†,‡]*

[†] Chemical Sciences and Engineering Division, Argonne National Laboratory, Lemont, IL, 60439, USA

[‡] Joint Center for Energy Storage Research, Argonne National Laboratory, Lemont, IL 60439, USA

[§] X-ray Science Division, Advanced Photon Source, Argonne National Laboratory, Lemont, IL 60439, USA

[ǀ] Department of Materials Science and Engineering, Research Institute of Advanced Materials (RIAM), Seoul National University, Seoul, 08826, Republic of Korea

[‖] Department of Physics, University of Illinois at Chicago, Chicago, IL 60607, USA

[#] Department of Chemistry and the Waterloo Institute for Nanotechnology, University of Waterloo, Waterloo, Ontario N2L 3G1, Canada

[Δ] Materials Science Division, Argonne National Laboratory, Lemont, IL 60439, USA

[⊥] Center for Nanoparticle Research, Institute for Basic Science (IBS), Seoul National University, Seoul 08826, Republic of Korea

[ζ] Institute of Engineering Research, College of Engineering, Seoul National University, Seoul 08826, Republic of Korea

Corresponding Authors

* E-mail: vaughey@anl.gov
lfnazar@uwaterloo.ca

ABSTRACT

Calcium-ion batteries (CIBs) are under investigation as next generation energy storage devices due to their theoretically high operating potentials and lower costs tied to the high natural abundance of calcium. However, the development of CIBs has been limited by the lack of available positive electrode materials. Here, for the first time, we report two functional polyanionic phosphate materials as high voltage cathodes for CIBs at room temperature. $NaV_2(PO_4)_3$ electrodes were found to reversibly intercalate 0.6 mol of Ca^{2+} (81 mA h g^{-1}) near 3.2 V (vs. Ca^{2+}/Ca) with stable cycling performance at a current density of 3.5 mA g^{-1}. The olivine framework material $FePO_4$ reversibly intercalates 0.2 mol of Ca^{2+} (72 mA h g^{-1}) near 2.9 V (vs. Ca^{2+}/Ca) at a current density of 7.5 mA g^{-1} in the first cycle. Structural, electronic, and compositional changes are consistent with reversible Ca^{2+} intercalation into these two materials.

TOC GRAPHICS

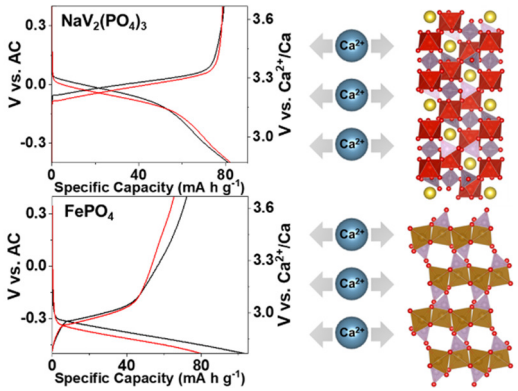

For nearly 30 years, energy storage systems based on lithium-ion intercalation have been the energy storage system of choice for numerous applications ranging from portable electronics to electric vehicles due to their high energy density and good cycle life.[1,2] However, the identification of new research pathways that may allow LIB technology to reach higher energy densities is limited, creating an opportunity for alternative cation-based chemistries that may overcome these limits.[3–5] Among these beyond-lithium chemistries, energy storage concepts based on multivalent-ions have received considerable attention as alternatives to LIBs as theoretically they have higher energy densities than LIBs when used in conjunction with metal anodes, as they have similar cell voltages and the multivalent transporting cation may yield higher capacities.[3–5] Among the many multivalent battery systems (Al^{3+}, Ca^{2+}, Mg^{2+}, Zn^{2+}) being considered, calcium-ion batteries (CIB) appear to be particularly promising as they provide the highest operating voltage among the multivalent systems due to the low Ca^{2+}/Ca reduction potential (−2.87 V vs. standard hydrogen electrode).[6,7] Furthermore, as Ca salts are generally nontoxic, abundant, and widely available, new systems may have cost and recycling benefits. However, the development of CIBs has remained in a nascent stage due to the lack of functional electrode materials and effective electrolytes that enable efficient calcium plating and stripping. This is highlighted by recent advances in calcium metal electrodeposition that represent a major step forward in the understanding of CIB anodes.[8–15] For continued CIB development, the discovery of high voltage calcium-ion cathode materials would be a major step towards improving our understanding and creating new insights to further the field of CIBs. Efforts to develop CIB cathodes have been made mainly based on established intercalation materials such as Prussian blue analogs[16–20] and layered materials ($VOPO_4 \cdot 2H_2O$[21], $Mg_{0.25}V_2O_5 \cdot H_2O$[22], MoO_3[23,24], V_2O_5[25], $Ca_{0.5}CoO_2$[26]). Although these early works helped establish the needed

materials design principles for future CIB studies, further improvements are necessary. For instance, Prussian Blue analogs are difficult to dehydrate and often have issues with salt co-intercalation, leading to low volumetric energy density.[27] Several layered oxide materials show significant capacitive behavior with large voltage hysteresis and without clear voltage plateaus during cycling probably due to a large overpotential.

The search for potential cathode insertion materials has been hampered by the relatively large ionic size of Ca^{2+} (e.g. Ca^{2+}: 114 pm, Na^{+}: 116 pm, Li^{+}: 90 pm) that limits its ability to fit into several common ionically conductive framework structures (i.e. spinel), the complex interfacial chemistry of multivalent cations, and high activation energy barrier originating from the divalent charge of Ca^{2+} ions.[6,7,28] In this light, three-dimensional (3D) structures built on redox active transition metals and polyanions $(XO_4)_n^-$ (X: P, Si, S), are promising candidates for Ca-ion battery electrodes. Such highly covalent three-dimensional frameworks can generate large stable interstitial spaces capable of supporting calcium insertion and extraction.[29–33] Higher cell voltages can also be achieved with the introduction of polyanion groups that increase the redox potential by the inductive effect.[29–31]

Here, we demonstrate two representative polyanion phosphates as new high voltage CIB cathodes. $NaV_2(PO_4)_3$ and $FePO_4$ were chosen as they are electrochemically active with sodium cations (Na^{+} (116 pm), which has a similar ionic radius to Ca^{2+} (114 pm)) and other studied multivalent intercalation cations (Zn^{2+}, Mg^{2+}, Al^{3+}).[34–41] In our study, we observed reversible calcium intercalation at high voltage at room temperature in a non-aqueous electrolyte. Importantly, we utilized numerous multiple characterization techniques, including synchrotron XRD, XAS, EELS, and EDS analysis to elucidate and confirm reversible calcium intercalation.

The polyanionic host materials, $NaV_2(PO_4)_3$ and $FePO_4$, were prepared by the electrochemical oxidation of $Na_3V_2(PO_4)_3$ and $LiFePO_4$, respectively. Vacant lattice sites for Ca^{2+} intercalation were created, via electrochemical removal of Na^+ and Li^+ from $Na_3V_2(PO_4)_3$ and $LiFePO_4$, respectively (Figure S1a and S2a). Specifically, $Na_3V_2(PO_4)_3$ was charged at 5 mA g^{-1} up to 0.5 V vs. activated carbon (AC) and $LiFePO_4$ was charged at 10 mA g^1 up to 0.6 V vs. AC, respectively, in 1 M $Ca(TFSI)_2$ in acetonitrile using an AC anode at room temperature (acetonitrile was only used for Na^+ and Li^+ removal). After charging, the electrodes were washed with fresh acetonitrile to remove any residual salt on the surface. Diglyme was chosen as the electrolyte solvent for the Ca intercalation reactions because of its good thermal stability, high salt solubility, and large potential window.[42,43] As the effort is focused on identifying and evaluating cathode materials (and to avoid possible CaF_2 passivation of a Ca metal anode), electrodes were tested against capacitive-type AC electrodes. The charging curve of $Na_3V_2(PO_4)_3$ (Figure S1a) showed a voltage plateau around 0.1 V vs. AC with a charge capacity of 108 mA h g^{-1} corresponding to 92 % theoretical capacity based on the expected endmember, $NaV_2(PO_4)_3$. $LiFePO_4$ showed similar behavior (Figure S2a) with a voltage plateau around -0.06 V vs. AC and a charge capacity of 159 mA h g^{-1} corresponding to 93.5 % of theoretical capacity, representing nearly complete Li^+ extraction in the electrochemical window. These data confirm that the potential of the AC electrode utilized is stable and functions well as a quasi-reference electrode.

To confirm the structure and purity of each phase, synchrotron XRD studies were performed on the pristine materials ($Na_3V_2(PO_4)_3$, $LiFePO_4$) and the charged samples ($NaV_2(PO_4)_3$, $FePO_4$) (see Figure S1b, S1c, S2b, and S2c). Refinement details are described in the supporting information while the refined lattice parameters of $Na_3V_2(PO_4)_3$ and $LiFePO_4$ at different states of charge obtained from Rietveld refinement are shown in Table 1.

Table 1. Refined unit cell dimensions (Rietveld refinements to synchrotron data) for $Na_3V_2(PO_4)_3$ and $LiFePO_4$ at different states of charge.

Charge State	Phase	a (Å)	b (Å)	c (Å)	α (°)	β (°)	γ (°)	V ($Å^{-3}$)	Space Group
Pristine	$Na_3V_2(PO_4)_3$	15.11409 (5)	8.73032(3)	8.82809(3)	90	124.539(2)	90	959.5549(7)	C2/c
Na Charged	$NaV_2(PO_4)_3$	8.42933(3)	8.42933(3)	21.4895(1)	90	90	120	1322.342(1)	$R\bar{3}c$
Ca Charged	$NaV_2(PO_4)_3$	8.42917(3)	8.42917(3)	21.4884(1)	90	90	120	1322.227(1)	$R\bar{3}c$
Pristine	$LiFePO_4$	10.32411(3)	6.00591(2)	4.6934(2)	90	90	90	291.019(2)	Pnma
Li Charged	$FePO_4$	9.82534(8)	5.79554(4)	4.78388(4)	90	90	90	272.4092(4)	Pnma
Ca Charged	$FePO_4$	9.81763(8)	5.79273(4)	4.7836(4)	90	90	90	272.0475(4)	Pnma

The synthesized $NaV_2(PO_4)_3$ and $FePO_4$ materials were investigated as Ca ion intercalation hosts by galvanostatic discharge/charge studies at constant current densities of 3.5 mA g^{-1} ($NaV_2(PO_4)_3$) and 7.5 mA g^{-1} ($FePO_4$) in 0.5 M $Ca(TFSI)_2$ in diglyme using an AC anode at room temperature (Figure 1). The voltage calibration with respect to voltage vs. Ca^{2+}/Ca is described in the experimental section in the Supporting Information. In Figure 1a, it is demonstrated that the $NaV_2(PO_4)_3$ electrode in this electrochemical system exhibits a highly reversible first discharge and charge capacities of 81 and 79 mA h g^{-1}, corresponding to 0.608 mol of $Ca^{2+}/NaV_2(PO_4)_3$ (charge capacity basis). The discharge-charge curves of the $Ca_x[NaV_2(PO_4)_3]$ electrode show a voltage plateau around 3.2 V vs. Ca^{2+}/Ca consistent with Ca intercalation and deintercalation. Based on the calibration studies, the observed reversible insertion reaction voltage is generally higher than that seen for other well studied multivalent chemistry systems and confirms the promise of polyanion cathodes in Ca-ion systems (Table S1). The dQ/dV profile has redox peaks at 3.25 V and 3.29 V vs. Ca^{2+}/Ca, corresponding to a hysteresis of only 0.04 V. This value is the smallest we are aware of for CIB electrodes and

represents one of the first multivalent-based energy storage systems with such highly reversible reaction kinetics and small interfacial problems.[44,45] In addition to the NASICON framework, the $FePO_4$ olivine electrode was found to exhibit capacities of 103 and 72 mA h g^{-1} for the first discharge and charge, respectively, a 30 % drop in reversible capacity on the first cycle. The differences in the materials that may cause such changes to be manifested will be discussed later in the discussion (Figure 1b). For the olivine, the charge capacity corresponds to 40.5 % of the theoretical value (based on the mass of $FePO_4$) or ~0.2 mol Ca^{2+} per $FePO_4$. The $FePO_4$ electrodes also showed voltage plateaus near 2.9 V (vs. Ca^{2+}/Ca) in the discharge-charge curves, similar to value seen in $Ca_x[NaV_2(PO_4)_3]$, and consistent with the values expected for Ca^{2+} intercalation/deintercalation based on reported Na_x[FePO4] studies.[37] The redox peak potentials in the dQ/dV curves are 3.04 and 3.15 V (vs. Ca^{2+}/Ca), with a hysteresis of 0.11 V.

The cycling performance of the $NaV_2(PO_4)_3$ and $FePO_4$ host electrodes were investigated at room temperature at constant current densities of 3.5 mA g^{-1} ($NaV_2(PO_4)_3$) and 7.5 mA g^{-1} ($FePO_4$). (Figure 1c and 1d) The $NaV_2(PO_4)_3$ electrode delivered a reversible and relatively stable discharge capacity of 83 mA h g^{-1} after 40 cycles, indicating good capacity retention and a stable framework. In contrast, $FePO_4$ showed significant capacity decay. Based on literature reports, the cycling performance of Mg-ion olivine cathodes in glyme electrolytes has been reported to also have higher capacity fade than expected probably due to either impedance increases, or cation trapping side reactions associated with surface degradation reactions.[46]

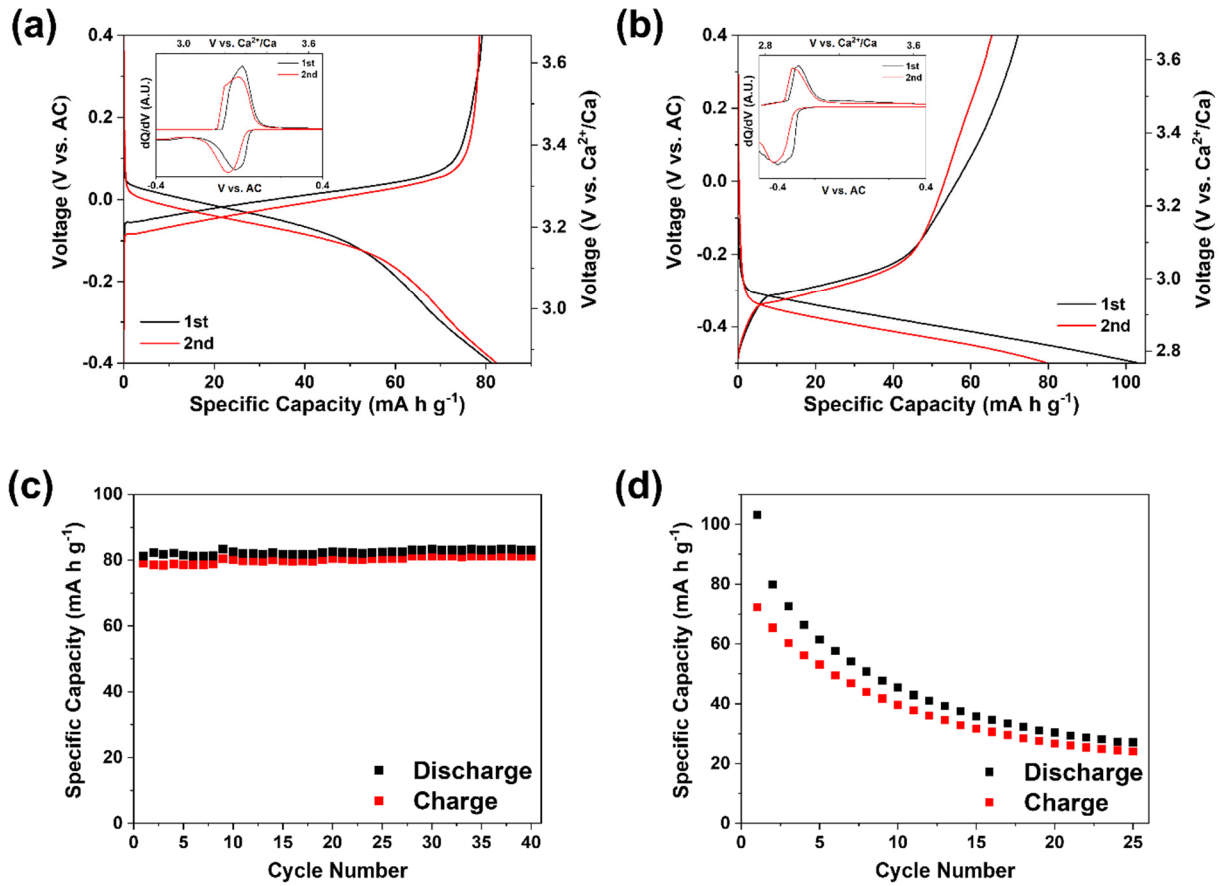

Figure 1. 1st and 2nd cycle galvanostatic discharge-charge curves of (a) $NaV_2(PO_4)_3$ at 3.5 mA g^{-1} and (b) $FePO_4$ at 7.5 mA g^{-1} at room temperature. The insets show the corresponding differential capacity plots. Cycling performance of (c) $NaV_2(PO_4)_3$ at 3.5 mA g^{-1} and (d) $FePO_4$ at 7.5 mA g^{-1} at room temperature.

As in many of these complex multivalent battery systems, several reported early studies were based on inadvertent mixtures of cations, proton involvement, or simply corrosion reactions mimicking the desired electrochemical activity. With this history and a paucity of Ca-specific spectroscopic detection techniques commonly available, e.g. ^{43}Ca MAS-NMR, it is necessary to confirm the transporting species and their nature to gain insights into the energy storage mechanism involved. To ensure that Ca^{2+} intercalation is the predominant electrochemical reaction for $NaV_2(PO_4)_3$ and $FePO_4$ frameworks, ex-situ synchrotron XRD data of discharged and charged electrodes were collected and studied. The diffraction patterns, shown in Figure 2,

were normalized to the highest peak intensity of the active materials to compensate for particle size differences and materials processing artifacts. Reversible structural changes were observed for both $NaV_2(PO_4)_3$ and $FePO_4$ upon cycling consistent with changes in the diffraction pattern and lattice versus state of charge. In the diffraction pattern of discharged $NaV_2(PO_4)_3$, seen in Figure 2a (middle), a new set of diffraction peaks appear on the lower angle side of each peak of the $NaV_2(PO_4)_3$ phase, consistent with lattice expansion and intercalation of Ca^{2+}. Fully resolving these new larger unit cell phases was not possible due to the significant overlap of peaks belonging to these closely related multiple phases. A possible monoclinic distortion upon reduction, as noted in the fully sodiated phase $Na_3V_2(PO_4)_3$, increased the difficulty of a definitive phase identification from the data. The formation of a complex mixture of related new phases is consistent with isolation of various metastable phases in the system derived from partial vacancy/Ca^{2+} ordering due to slow Ca^{2+} diffusion[23,47] or possibly Na^+/Ca^{2+} re-ordering[41,48]. Although not evaluated fully to date, the use of longer equilibration times, voltage holds, or higher temperatures may resolve some of the structural issues associated with these metastable phases. Its implication on the Ca-ion insertion mechanism will be discussed after the data from the XAS studies is presented. DFT (density functional theory) calculations were performed (Figure 2b) on both $CaNaV_2(PO_4)_3$, and $Ca_{0.5}NaV_2(PO_4)_3$ in order to evaluate the cation diffusion pathway. The study indicated that the most energetically favorable state involved some cation mixing over the two possible crystallographic sites (6b, 18e). Although consistent with previous NASICON cation diffusion pathway studies, our diffraction data was not of sufficient resolution to investigate this model.[41,50] Notably, after charging (Ca^{2+} removal) the $Ca_x[NaV_2(PO_4)_3]$ reduced phase, the XRD pattern of the initial charged $NaV_2(PO_4)_3$ phase is regenerated, demonstrating the high reversibility of Ca^{2+} intercalation/deintercalation in the

NASICON structure (Figure 2a and S4a and Table 1). This assessment is consistent with the high resolution XRD data in Figure 2a that show that small differences in Na/Ca stoichiometry or ordering are manifested as detectable changes in the patterns.

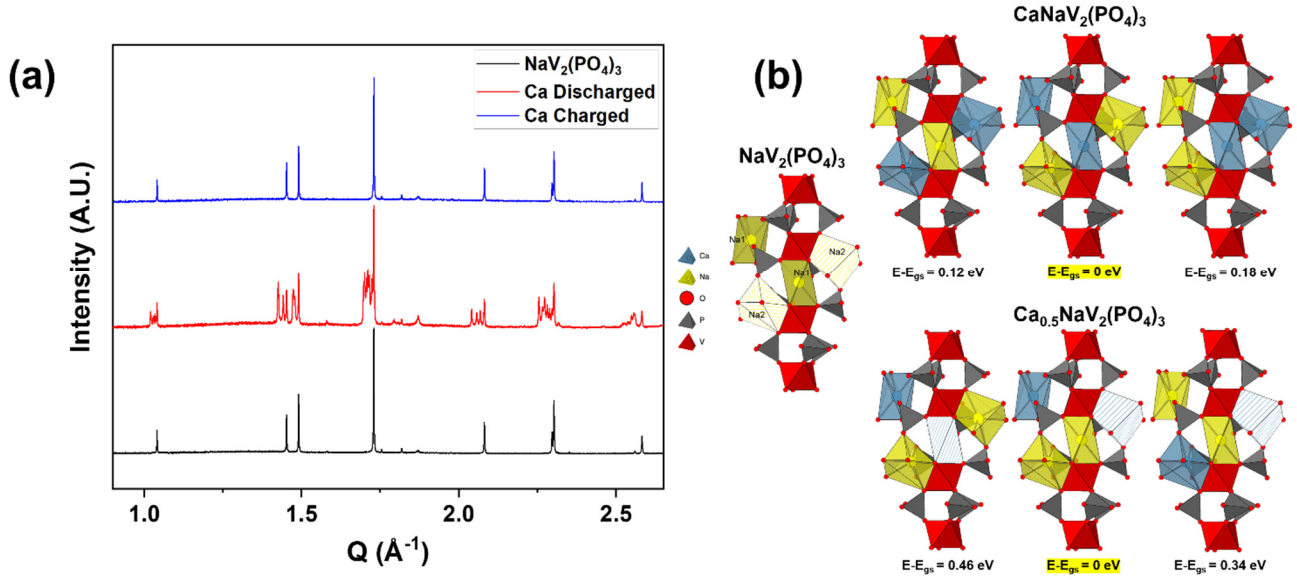

Figure 2. Ex situ synchrotron XRD patterns of (a) $NaV_2(PO_4)_3$ and (b) DFT-optimized structures of $NaV_2(PO_4)_3$, and $CaNaV_2(PO_4)_3$, and $Ca_{0.5}NaV_2(PO_4)_3$ with various Ca and Na sites.

In contrast to the $NaV_2(PO_4)_3$ NASICON studies, for $FePO_4$ only a single new orthorhombic phase was detected by high resolution XRD when the cathode was discharged in a Ca-ion electrolyte (Figure 3a). Both $FePO_4$ and a calciated $FePO_4$ phase were studied and compared using the diffraction data collected (Figure 3b). The initial refinements in space group Pnma suggested that Ca^{2+} ions were not occupying the Li site (from $LiFePO_4$) nor the crystallographic site (Pnma space group) identified in the sodium analogue ($NaFePO_4$).[37] As calcium cations are commonly observed in oxide coordination greater than six and as suggested by the Fourier map (see SI), the Ca^{2+} cation may prefer to occupy a site near (but not on) the original Li site (Figure 3c), unlike the Na analogue.[37] However, due to poor peak intensity at

high angle and significant overlapping peaks, the true location and fraction of the Ca^{2+} cation could not be refined with confidence. Rietveld refinement indicated mixed phases consistent with a weight ratio of $FePO_4$ to the calciated $FePO_4$ phase of approximately 55 to 45 %. After charging, the $FePO_4$ phase is completely recovered with similar peak widths to the initial diffraction pattern, indicating the good reversibility of Ca intercalation and deintercalation into the olivine structure (Figure 3a and S4b and Table 1). The diffraction and electrochemical evidence together suggest that the large (~30%) irreversible capacity shown in the first cycle probably does not arise from an incomplete charging reaction, e.g. electronic isolation of a $Ca_x[FePO_4]$ phase, but probably from electrolyte-based side reactions that are associated with surface degradation reactions that consume active Ca^{2+} that is thus unavailable to future cycles, similar to passivation layers in LIBs that trap lithium cations and contribute to poor coulombic efficiency.

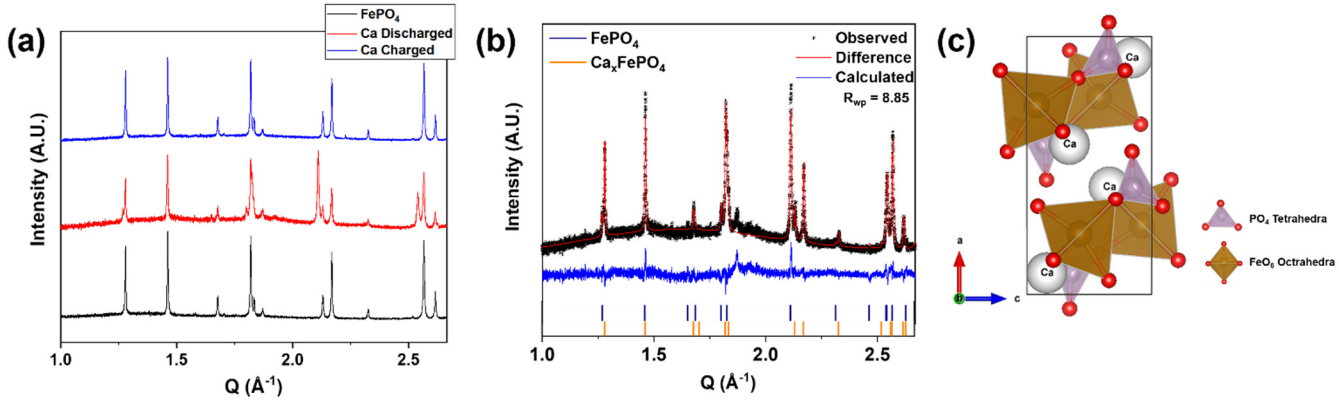

Figure 3. Ex situ synchrotron XRD patterns of (a) $FePO_4$ at different states of charge. (b) High resolution XRD data Rietveld refinement of calciated $FePO_4$. (c) Tentative Ca position in calciated $FePO_4$ suggested by Rietveld refinement. Possible distortions of the framework are not shown.

XAS was used to study changes in the local structure of the transition metal species (i.e the transition metal V, Fe sites) and verify changes in their oxidation state in response to calcium intercalation and deintercalation. Figures 4a and 4b show the V K-edge and Fe K-edge X-ray absorption near edge structure (XANES) spectra of $NaV_2(PO_4)_3$ and $FePO_4$, respectively, at different charge states during cycling. To first order, XANES data provide a bulk-averaged measure of the transition metal oxidation state and has been commonly used to study charge transfer in both Li-ion and multivalent battery chemistries.[49–51] The position of the main edge, corresponding to a 1s → 4p transition, is affected by the degree of screening of the transition metal valence electrons.[52,53] When the $NaV_2(PO_4)_3$ electrode was discharged, the V K-edge shifted approximately 2.5 eV towards lower energies due to the reduction of V^{4+} toward V^{3+} (Figure 4a). After charging, the V K-edge shifted back to the original position of $NaV_2(PO_4)_3$, consistent with oxidation to V^{4+}. The $FePO_4$ electrodes showed a similar tendency (Figure 4b). A reversible Fe K-edge shift was observed during cycling, indicating the reversible oxidation state change of Fe. However, the Fe K-edge had less of a relative shift than the V K-edge, consistent with less calcium insertion seen in the electrochemical and diffraction-based experiments. This agrees with the relative active material utilizations, where $NaV_2(PO_4)_3$ and $FePO_4$ delivered 60.5 and 40.5 % theoretical capacities, respectively.

The local environment around the transition metal atom (V, Fe) was also investigated using extended X-ray absorption fine structure (EXAFS) spectra at different states of charge (Figure 4c and 4d). The first peak in the Fourier-transformed EXAFS data is due to scattering from the nearest neighbor oxygen atoms. The amplitude of this peak decreased for both $NaV_2(PO_4)_3$ and $FePO_4$, suggesting the VO_6 and FeO_6 octahedral distortion upon calciation. After charging, the amplitude was recovered, indicating good reversibility of the local structure.

The valence states of the transition metals were studied by EELS, providing similar electronic structure information to XAS, but with atomic-scale spatial resolution. EELS was measured from the surface and bulk region of calciated $NaV_2(PO_4)_3$ and $FePO_4$. Figures 4e and 4f show the $L_{2,3}$-edges of the transition metals (V, Fe) originating from the excitation of 2p electrons to the unoccupied 3d states of the metals. The calciated $NaV_2(PO_4)_3$ showed the V L_3-edge peak at 517 eV from the surface which is the characteristic peak of V^{3+}.[54,55] On the other hand, two V L_3-edge peaks from the bulk were observed at 517 eV and 518.35 eV, indicating the bulk region consists of both V^{3+} and V^{4+} considering the high energy peak represents a higher oxidation state.[55] The calciated $FePO_4$ showed a similar trend. The Fe L_3-edge from the surface showed a peak at 707.05 eV and the Fe L_3-edge from the bulk shifted to higher energy by ~1.5 eV compared to the surface, indicating that the oxidation state of Fe at the surface is 2+ while Fe^{3+} is dominant in the bulk.[56] In summary, the reduced valence states of transition metals due to calciation were confirmed by EELS but the oxidation state was not found to be uniform starting from the surface and moving to the bulk (core). Because both XAS and XRD studies indicate that Ca^{2+} intercalation did not occur uniformly across the active materials and both types of materials tested below theoretical capacity under the conditions used in this study, the working model postulated for these partially calciated discharged products is an active particle with a calcium-rich surface relative to the bulk composition. Further materials optimization studies, including nanoscale synthesis of the cathodes to give a shorter Ca diffusion length and using a higher temperature cell testing protocol to increase the diffusion rate, may increase the uniformity of the particle and unite the surface and bulk compositions. In preliminary testing, cycling the $FePO_4$ electrode in Ca-ion electrolytes at 50 °C did show a higher specific capacity (Figure S5) and will be investigated in future efforts.

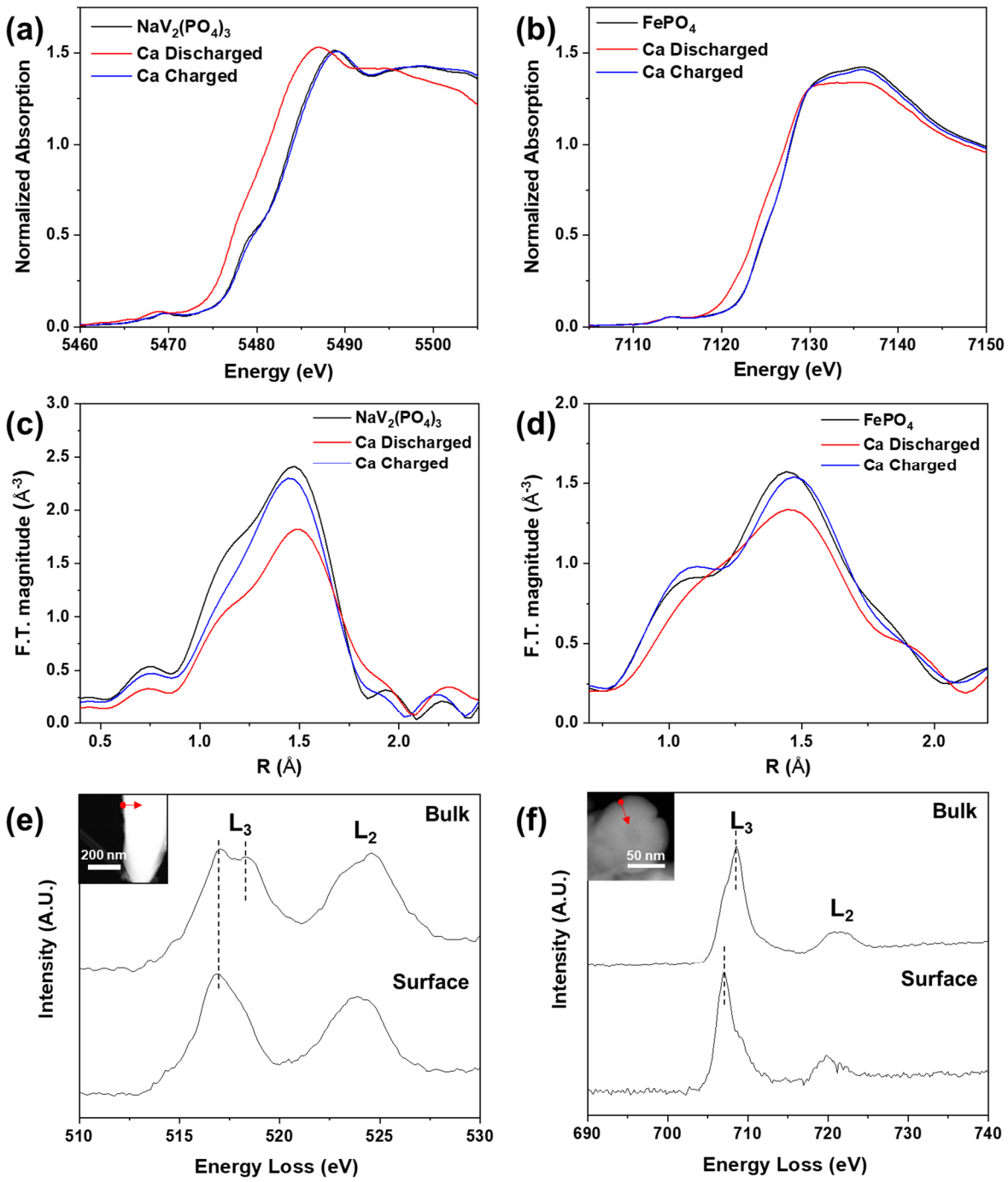

Figure 4. Ex situ (a) V K-edge XANES spectra of $NaV_2(PO_4)_3$ and (b) Fe K-edge XANES spectra of $FePO_4$ at different states of charge. Ex situ (c) V K-edge EXAFS spectra of $NaV_2(PO_4)_3$ and (d) Fe K-edge EXAFS spectra of $FePO_4$ at different states of charge (phase is not corrected). EELS spectra of (e) calciated $NaV_2(PO_4)_3$ and (f) calciated $FePO_4$. The insets show the EELS acquisition area indicating the direction from the surface to bulk. 10 nm from the edge of the particle is considered as a threshold for surface and bulk.

To track the calcium-ions in the system, EDS studies were carried out to quantify the amount of Ca insertion and extraction during cycling (Figure 5a and 5b). Using $NaV_2(PO_4)_3$ and $FePO_4$ electrodes that were washed thoroughly with acetonitrile to ensure that no calcium electrolyte salt residue remained on the surface (experimentally no electrolyte components, notably sulfur atom from the salt $TFSI^-$ anion was detected). EDS spectra were normalized to the transition metal signal (V, Fe). The $NaV_2(PO_4)_3$ electrode showed distinct Ca signals at 3.7 keV for Ca Kα and 4.0 keV for Ca Kβ after discharge. After charging, the Ca signal was significantly diminished relative to the metals, indicating Ca deintercalation. The $FePO_4$ electrode showed similar behavior, but with more residual Ca in the spectra relative to the metals in the framework, probably related to the higher first cycle irreversible capacity losses (Figure S4b and Table 1). The amount of Ca in $NaV_2(PO_4)_3$ and $FePO_4$ electrodes based on the EDS quantification results and calculated from the discharge and charge capacity of EDS samples are shown in Figure 5c and are in rough agreement with the values determined from the electrochemical studies. Mechanistically, an important outcome of the EDS study beside confirmation of calcium cycling, was that the Na content did not change significantly during the electrochemical cycling, including a comparison of a Ca-ion electrolyte cycled $NaV_2(PO_4)_3$ and the uncycled $NaV_2(PO_4)_3$. This is consistent with Ca ions being the active transporting species and the sodium, under the testing conditions used, being electrochemically inaccessible. This trapping of sodium is also consistent with synthesis of the simple $V_2(PO_4)_3$ NASICON framework which cannot be isolated from $Na_3V_2(PO_4)_3$ (it can only be prepared chemically starting from the lithium analogue, using an NO_2BF_4 /AN solution under nitrogen.[57]). We expect some discrepancy in the EDS results is due to different sample and measurement conditions and complexity of the sample containing a large amount of carbon, binder, and current collector. Nonetheless, the data clearly show that

reversible Ca intercalation in both $NaV_2(PO_4)_3$ and $FePO_4$ occurs, which is consistent with the evidence from the other complementary characterization methods.

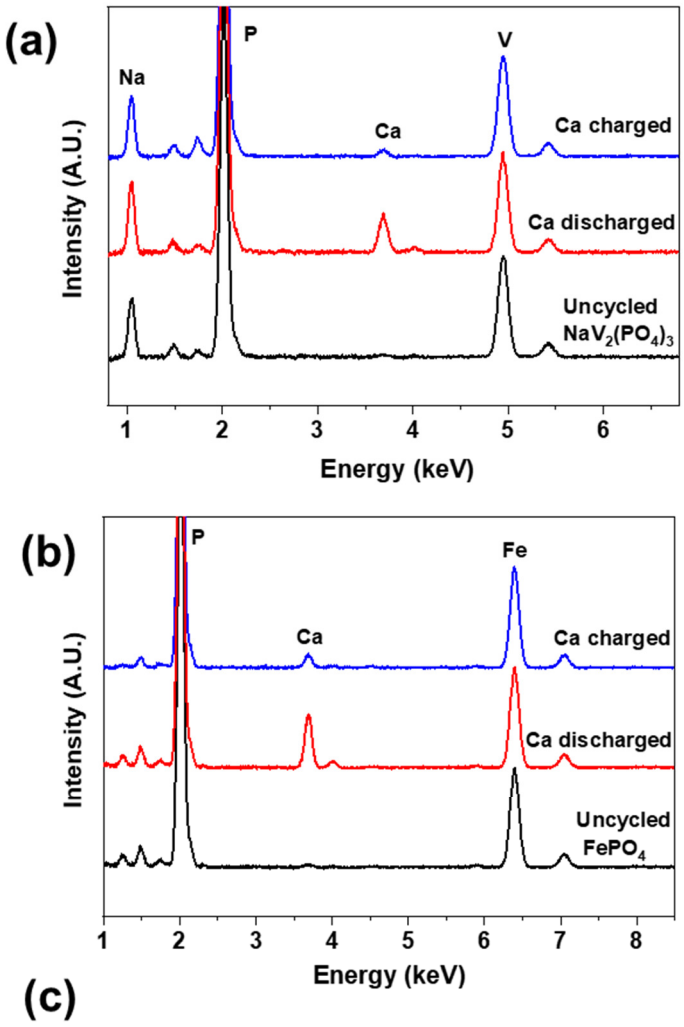

(c)

	$NaV_2(PO_4)_3$			$FePO_4$	
	Na (mol)	Ca (mol)		Ca (mol)	
		EDS	Echem	EDS	Echem
Ca discharged	0.86	0.5	0.58	0.21	0.27
Ca charged	0.80	undetectable	0.01	0.05	0.08

Figure 5. Ex situ EDS spectra of (a) $NaV_2(PO_4)_3$ and (b) $FePO_4$ before cycling and after discharge and charge in Ca cells. (c) EDS results for $NaV_2(PO_4)_3$ and $FePO_4$.

In conclusion, we report on two polyanionic phosphates, the NASICON-type $NaV_2(PO_4)_3$ and the olivine-type $FePO_4$, and they were studied as CIB cathodes at room temperature in a non-aqueous electrolyte for the first time. Both $NaV_2(PO_4)_3$ and $FePO_4$ can reversibly intercalate Ca^{2+} in a cell that uses a capacitive AC anode at a high voltage vs. Ca^{2+}/Ca glyme based electrolyte. Based on synchrotron XRD, XAS, EELS and EDS results, we have confirmed that Ca can be intercalated into and deintercalated from the sodium stabilized NASICON framework material $NaV_2(PO_4)_3$ (0.6 mol of Ca^{2+}) with stable cyclability for over 40 cycles. In contrast, the olivine material $FePO_4$ (0.2 mol of Ca^{2+}) cycles but suffers from capacity decay probably due to side reactions on the surface that consume active calcium-ions in the electrolyte which is consistent with the diffraction data that shows retention of framework integrity and crystallinity on cycling. The $NaV_2(PO_4)_3$ cathode exhibited an initial discharge capacity of 81 mA h g^{-1} at 3.5 mA g^{-1} with a discharge plateau around 3.2 V vs. Ca^{2+}/Ca. The $FePO_4$ cathode showed an initial discharge capacity of 103 mA h g^{-1} at 7.5 mA g^{-1} at room temperature with a discharge plateau around 2.9 V vs. Ca^{2+}/Ca. Both $NaV_2(PO_4)_3$ and $FePO_4$ showed well defined voltage plateaus and a small voltage hysteresis ($NaV_2(PO_4)_3$: 0.04 V, $FePO_4$: 0.11 V), making the NASICON notably, a possible candidate for future CIB full cell development as the next generation of anode materials are developed. Future studies will identify conditions to further improve cyclability. We also report that both $NaV_2(PO_4)_3$ and $FePO_4$ lattices insert calcium ions using different Ca intercalation mechanisms compared to either of their Na and Li analogs and demonstrate good structural stability during Ca^{2+} intercalation and deintercalation. We believe that this work demonstrates that polyanion phosphates are promising host candidates for CIBs and will spur further research on polyanionic phosphates as electrode materials for CIBs.

ASSOCIATED CONTENT

Supporting Information

The Supporting Information is available free of charge at:

Experimental methods and additional figures and tables: Electrochemical data, XRD patterns, and Rietveld refinement of ex situ samples, crystal structure, magnified XRD patterns, electrochemical data at elevated temperature, SEM, voltage calibration, voltage comparison with other multivalent chemistry systems, refined parameters of ex situ samples.

AUTHOR INFORMATION

Corresponding Author

* E-mail: vaughey@anl.gov

Notes

The authors declare no competing financial interest.

ACKNOWLEDGMENT

This work was supported by the Joint Center for Energy Storage Research, an Energy Innovation Hub funded by the U.S. Department of Energy, Office of Science, Basic Energy Sciences. This research used resources of the Advanced Photon Source, a U.S. Department of Energy (DOE) Office of Science User Facility operated for the DOE Office of Science by Argonne National Laboratory under Contract No. DE-AC02-06CH11357. This work is conducted at Argonne National Laboratory supported by the U.S. Department of Energy under contract DE-A02-06CH11357. The acquisition of JEOL JEM ARM200CF at the University of Illinois at Chicago was supported by an MRI-R2 grant from the National Science Foundation (Grant No. DMR-0959470) and the upgraded Gatan Continuum spectrometer was supported by a grant from the NSF (DMR-1626065).

REFERENCES

1. Etacheri, V.; Marom, R.; Elazari, R.; Salitra, G.; Aurbach, D. Challenges in the development of advanced Li-ion batteries: a review. *Energy Environ. Sci*. **2011,** *4,* 3243–3262.

2. Blomgren, G. E. The Development and Future of Lithium Ion Batteries. *J. Electrochem. Soc.* **2016,** *164*, A5019–A5025.

3. Ponrouch, A.; Bitenc, J.; Dominko, R.; Lindahl, N.; Johansson, P.; Palacin, M. R. Multivalent rechargeable batteries. *Energy Storage Mater.* **2019,** *20*, 253–262.

4. Liu, M.; Rong, Z.; Malik, R.; Canepa, P.; Jain, A.; Ceder, G.; Persson, K. A. Spinel compounds as multivalent battery cathodes: a systematic evaluation based on ab initio calculations. *Energy Environ. Sci*. **2015,** *8*, 964–974.

5. Canepa, P.; Sai Gautam, G.; Hannah, D. C.; Malik, R.; Liu, M.; Gallagher, K. G.; Persson, K. A.; Ceder, G. Odyssey of Multivalent Cathode Materials: Open Questions and Future Challenges. *Chem. Rev.* **2017,** *117*, 4287−4341.

6. Ponrouch, A.; Palacin, M. R. On the road toward calcium-based batteries. *Curr. Opin. Electrochem.* **2018,** *9*, 1−7.

7. Gummow, R. J.; Vamvounis, G.; Kannan, M. B.; He, Y. Calcium-Ion Batteries: Current State-of-the-Art and Future Perspectives. *Adv. Mater.* **2018,** *30*, e1801702.

8. Ponrouch, A.; Frontera, C.; Barde, F.; Palacin, M. R. Towards a calcium-based rechargeable battery. *Nat. Mater.* **2016,** *15*, 169−72.

9. Wang, D.; Gao, X.; Chen, Y.; Jin, L.; Kuss, C.; Bruce, P. G. Plating and stripping calcium in an organic electrolyte. *Nat. Mater.* **2018,** *17*, 16−20.

10. Li, Z.; Fuhr, O.; Fichtner, M.; Zhao-Karger, Z. Towards stable and efficient electrolytes for room-temperature rechargeable calcium batteries. *Energy Environ. Sci*. **2019,** *12*, 3496−3501.

11. Ta, K.; Zhang, R.; Shin, M.; Rooney, R. T.; Neumann, E. K.; Gewirth, A. A. Understanding Ca Electrodeposition and Speciation Processes in Nonaqueous Electrolytes for Next-Generation Ca-Ion Batteries. *ACS Appl. Mater. Interfaces* **2019,** *11*, 21536−21542.

12. Shyamsunder, A.; Blanc, L. E.; Assoud, A.; Nazar, L. F. Reversible Calcium Plating and Stripping at Room Temperature Using a Borate Salt. *ACS Energy Lett.* **2019,** *4*, 2271−2276.

13. Park, J.; Xu, Z. L.; Yoon, G.; Park, S. K.; Wang, J.; Hyun, H.; Park, H.; Lim, J.; Ko, Y. J.; Yun, Y. S.; Kang, K. Stable and High-Power Calcium-Ion Batteries Enabled by Calcium Intercalation into Graphite. *Adv. Mater.* **2020,** *32*, e1904411.

14. Richard Prabakar, S. J.; Ikhe, A. B.; Park, W. B.; Chung, K. C.; Park, H.; Kim, K. J.; Ahn, D.; Kwak, J. S.; Sohn, K. S.; Pyo, M. Graphite as a Long-Life Ca^{2+}-Intercalation Anode

and its Implementation for Rocking-Chair Type Calcium-Ion Batteries. *Adv. Sci.* **2019,** *6*, 1902129.

15. Wang, M.; Jiang, C.; Zhang, S.; Song, X.; Tang, Y.; Cheng, H. M. Reversible calcium alloying enables a practical room-temperature rechargeable calcium-ion battery with a high discharge voltage. *Nat. Chem.* **2018,** *10*, 667−672.

16. Lipson, A. L.; Pan, B.; Lapidus, S. H.; Liao, C.; Vaughey, J. T.; Ingram, B. J. Rechargeable Ca-Ion Batteries: A New Energy Storage System. *Chem. Mater.* **2015,** *27*, 8442−8447.

17. Tojo, T.; Sugiura, Y.; Inada, R.; Sakurai, Y. Reversible Calcium Ion Batteries Using a Dehydrated Prussian Blue Analogue Cathode. *Electrochim. Acta* **2016,** *207*, 22−27.

18. Adil, M.; Dutta, P. K.; Mitra, S. An Aqueous Ca-ion Full Cell Comprising BaHCF Cathode and MCMB Anode. *Chem. Select.* **2018,** *3*, 3687−3690.

19. Adil, M.; Sarkar, A.; Roy, A.; Panda, M. R.; Nagendra, A.; Mitra, S. Practical Aqueous Calcium-Ion Battery Full-Cells for Future Stationary Storage. *ACS Appl. Mater. Interfaces* **2020,** *12*, 11489−11503.

20. Vo, T. N.; Hur, J.; Kim, I. T. Enabling High Performance Calcium-Ion Batteries from Prussian Blue and Metal–Organic Compound Materials. *ACS Sust. Chem. Eng.* **2020,** *8*, 2596−2601.

21. Wang, J.; Tan, S.; Xiong, F.; Yu, R.; Wu, P.; Cui, L.; An, Q. $VOPO_4 \cdot 2H_2O$ as a new cathode material for rechargeable Ca-ion batteries. *Chem. Commun.* **2020,** *56*, 3805−3808.

22. Xu, X.; Duan, M.; Yue, Y.; Li, Q.; Zhang, X.; Wu, L.; Wu, P.; Song, B.; Mai, L. Bilayered $Mg_{0.25}V_2O_5 \cdot H_2O$ as a Stable Cathode for Rechargeable Ca-Ion Batteries. *ACS Energy Lett.* **2019,** *4*, 1328−1335.

23. Cabello, M.; Nacimiento, F.; Alcántara, R.; Lavela, P.; Pérez Vicente, C.; Tirado, J. L. Applicability of Molybdite as an Electrode Material in Calcium Batteries: A Structural Study of Layer-type Ca_xMoO_3. *Chem. Mater.* **2018,** *30*, 5853−5861.

24. Tojo, T.; Tawa, H.; Oshida, N.; Inada, R.; Sakurai, Y. Electrochemical characterization of a layered α-MoO_3 as a new cathode material for calcium ion batteries. *J. Electroanal. Chem.* **2018,** *825*, 51−56.

25. Hayashi, M.; Arai, H.; Ohtsuka, H.; Sakurai, Y. Electrochemical insertion/extraction of calcium ions using crystalline vanadium oxide. *Electrochem. Solid-State Lett.* **2004**, *7*, A119−A121.

26. Cabello, M.; Nacimiento, F.; González, J. R.; Ortiz, G.; Alcántara, R.; Lavela, P.; Pérez-Vicente, C.; Tirado, J. L. Advancing towards a veritable calcium-ion battery: $CaCo_2O_4$ positive electrode material. *Electrochem. Commun.* **2016,** *67*, 59-64.

27. Hurlbutt, K.; Wheeler, S.; Capone, I.; Pasta, M. Prussian Blue Analogs as Battery Materials. *Joule* **2018,** *2*, 1950−1960.

28. Rong, Z.; Malik, R.; Canepa, P.; Sai Gautam, G.; Liu, M.; Jain, A.; Persson, K.; Ceder, G. Materials Design Rules for Multivalent Ion Mobility in Intercalation Structures. *Chem. Mater.* **2015,** *27*, 6016−6021.

29. Masquelier, C.; Croguennec, L. Polyanionic (phosphates, silicates, sulfates) frameworks as electrode materials for rechargeable Li (or Na) batteries. *Chem. Rev.* **2013,** *113*, 6552−6591.

30. Ni, Q.; Bai, Y.; Wu, F.; Wu, C. Polyanion-Type Electrode Materials for Sodium-Ion Batteries. *Adv. Sci.* **2017,** *4*, 1600275.

31. Gong, Z.; Yang, Y. Recent advances in the research of polyanion-type cathode materials for Li-ion batteries. *Energy Environ. Sci*. **2011,** *4*, 3223−3242.

32. Huang, Z.-D.; Masese, T.; Orikasa, Y.; Mori, T.; Yamamoto, K. Vanadium phosphate as a promising high-voltage magnesium ion (de)-intercalation cathode host. *RSC Adv.* **2015,** *5*, 8598−8603.

33. Rubio, S.; Liu, R.; Liu, X.; Lavela, P.; Tirado, J. L.; Li, Q.; Liang, Z.; Ortiz, G. F.; Yang, Y. Exploring the high-voltage Mg^{2+}/Na^{+} co-intercalation reaction of $Na_3VCr(PO_4)_3$ in Mg-ion batteries. *J. Mat. Chem. A* **2019,** *7*, 18081−18091.

34. Shan, P.; Gu, Y.; Yang, L.; Liu, T.; Zheng, J.; Pan, F. Olivine $FePO_4$ Cathode Material for Rechargeable Mg-Ion Batteries. *Inorg. Chem.* **2017,** *56*, 13411−13416.

35. Zeng, J.; Yang, Y.; Lai, S.; Huang, J.; Zhang, Y.; Wang, J.; Zhao, J. A Promising High-Voltage Cathode Material Based on Mesoporous $Na_3V_2(PO_4)_3$/C for Rechargeable Magnesium Batteries. *Chem. Eur. J.* **2017,** *23*, 16898−16905.

36. Nacimiento, F.; Cabello, M.; Alcántara, R.; Lavela, P.; Tirado, J. L. NASICON-type $Na_3V_2(PO_4)_3$ as a new positive electrode material for rechargeable aluminium battery. *Electrochim. Acta* **2018,** *260*, 798−804.

37. Moreau, P.; Guyomard, D.; Gaubicher, J.; Boucher, F. Structure and Stability of Sodium Intercalated Phases in Olivine $FePO_4$. *Chem. Mater.* **2010,** *22*, 4126−4128.

38. Zeng, J.; Wu, D.; Wang, X.; Wu, J.; Li, J.; Wang, J.; Zhao, J. Insights into the Mg storage property and mechanism based on the honeycomb-like structured $Na_3V_2(PO_4)_3$/C/G in anhydrous electrolyte. *Chem. Eng. J.* **2019,** *372*, 37−45.

39. Aragón, M. J.; Lavela, P.; Recio, P.; Alcántara, R.; Tirado, J. L. On the influence of particle morphology to provide high performing chemically desodiated $C@NaV_2(PO_4)_3$ as cathode for rechargeable magnesium batteries. *J. Electroanal. Chem.* **2018,** *827*, 128−136.

40. Li, G.; Yang, Z.; Jiang, Y.; Jin, C.; Huang, W.; Ding, X.; Huang, Y. Towards polyvalent ion batteries: A zinc-ion battery based on NASICON structured $Na_3V_2(PO_4)_3$. *Nano Energy* **2016,** *25*, 211−217.

41. Ko, J. S.; Paul, P. P.; Wan, G.; Seitzman, N.; DeBlock, R. H.; Dunn, B. S.; Toney, M. F.; Nelson Weker, J. NASICON $Na_3V_2(PO_4)_3$ Enables Quasi-Two-Stage Na^+ and Zn^{2+} Intercalation for Multivalent Zinc Batteries. *Chem. Mater.* **2020,** *32*, 3028−3035.

42. Ha, S. Y.; Lee, Y. W.; Woo, S. W.; Koo, B.; Kim, J. S. Cho, J.; Lee, K. T.; Choi, N. S. Magnesium(II) bis(trifluoromethane sulfonyl) imide-based electrolytes with wide electrochemical windows for rechargeable magnesium batteries. *ACS Appl. Mater. Interfaces* **2014,** *6*, 4063−4073.

43. Shao, Y.; Liu, T.; Li, G.; Gu, M.; Nie, Z.; Engelhard, M.; Xiao, J.; Lv, D.; Wang, C.; Zhang, J. G.; Liu, J. Coordination chemistry in magnesium battery electrolytes: how ligands affect their performance. *Sci. Rep.* **2013,** *3*, 3130.

44. Kwon, B. J.; Lau, K.-C.; Park, H.; Wu, Y. A.; Hawthorne, K. L.; Li, H.; Kim, S.; Bolotin, I. L.; Fister, T. T.; Zapol, P.; Klie, R. F.; Cabana, J.; Liao, C.; Lapidus, S. H.; Key, B.; Vaughey, J. T. Probing Electrochemical Mg-Ion Activity in $MgCr_{2-x}V_xO_4$ Spinel Oxides. *Chem. Mater.* **2019,** *32*, 1162−1171.

45. Tchitchekova, D. S.; Ponrouch, A.; Verrelli, R.; Broux, T.; Frontera, C.; Sorrentino, A.; Bardé, F.; Biskup, N.; Arroyo-de Dompablo, M. E.; Palacín, M. R. Electrochemical Intercalation of Calcium and Magnesium in TiS_2: Fundamental Studies Related to Multivalent Battery Applications. *Chem. Mater.* **2018,** *30*, 847−856.

46. Zhang, R.; Ling, C. Unveil the Chemistry of Olivine $FePO_4$ as Magnesium Battery Cathode. *ACS Appl. Mater. Interfaces* **2016,** *8*, 18018−18026.

47. Hubaud, A. A.; Schroeder, D. J.; Key, B.; Ingram, B. J.; Dogan, F.; Vaughey, J. T. Low temperature stabilization of cubic ($Li_{7-x}Al_{x/3}$)$La_3Zr_2O_{12}$: role of aluminum during formation. *J. Mater. Chem. A* **2013,** *1*, 8813−8818

48. Wang, Q.; Zhang, M.; Zhou, C.; Chen, Y. Concerted Ion-Exchange Mechanism for Sodium Diffusion and Its Promotion in $Na_3V_2(PO_4)_3$ Framework. *J. Phys. Chem. C* **2018,** *122*, 16649−16654.

49. Lipson, A. L.;Kim, S.; Pan, B.; Liao, C.; Fister, T. T.; Ingram, B. J. Calcium intercalation into layered fluorinated sodium iron phosphate. *J. Power Sources* **2017,** *369*, 133−137.

50. Yoo, H. D.; Jokisaari, J. R.; Yu, Y.-S.; Kwon, B. J.; Hu, L.; Kim, S.; Han, S.-D.; Lopez, M.; Lapidus, S. H.; Nolis, G. M. Intercalation of Magnesium into a Layered Vanadium Oxide with High Capacity. *ACS Energy Lett.* **2019**, *4*, 1528−1534.

51. Bak, S. M.; Shadike, Z.; Lin, R.; Yu, X.; Yang, X. Q. In Situ /Operando Synchrotron-Based X-Ray Techniques for Lithium-Ion Battery Research. *NPG Asia Mater.* **2018**, *10*, 563−580.

52. Horrocks, G. A.; Braham, E. J.; Liang, Y.; De Jesus, L. R.; Jude, J.; Velázquez, J. M.; Prendergast, D.; Banerjee, S. Vanadium K-Edge X-ray Absorption Spectroscopy as a Probe of the Heterogeneous Lithiation of V_2O_5: First-Principles Modeling and Principal Component Analysis. *J. Phys. Chem. C* **2016,** *120*, 23922−23932.

53. Ali, G.; Lee, J. H.; Susanto, D.; Choi, S. W.; Cho, B. W.; Nam, K. W.; Chung, K. Y. Polythiophene-Wrapped Olivine $NaFePO_4$ as a Cathode for Na-Ion Batteries. *ACS Appl. Mater. Interfaces* **2016,** *8*, 15422−15429.

54. Gloter, A.; Serin, V.; Turquat, C.; Cesari, C.; Leroux, C.; Nihoul, G. Vanadium valency and hybridization in V-doped hafnia investigated by electron energy loss spectroscopy. *Eur. Phys. J. B* **2001**, *22*, 179-186.

55. Yu, M.; Zeng, Y.; Han, Y.; Cheng, X.; Zhao, W.; Liang, C.; Tong, Y.; Tang, H.; Lu, X. Valence-Optimized Vanadium Oxide Supercapacitor Electrodes Exhibit Ultrahigh Capacitance and Super-Long Cyclic Durability of 100000 Cycles. *Adv. Funct. Mater.* **2015,** *25*, 3534–3540.

56. Chueh, Y. L.; Lai, M. W.; Liang, J. Q.; Chou, L. J.; Wang, Z. L. Systematic Study of the Growth of Aligned Arrays of α-Fe_2O_3 and Fe_3O_4 Nanowires by a Vapor–Solid Process. *Adv. Funct. Mater.* **2006,** *16*, 2243–2251.

57. Park, M. J.; Yaghoobnejad Asl, H.; Therese, S.; Manthiram, A. Structural Impact of Zn-Insertion into Monoclinic $V_2(PO_4)_3$: Implications for Zn-Ion Batteries. *J. Mater. Chem. A* **2019**, *7*, 7159–7167.